RESEARCH PAPER

Green Synthesis of $Ni_xMn_{1-x}Fe_2O_4$ Nanoparticles and Their Photocatalyst Studies Under the UV Irradiation

Tavus Hosseinabad [1], Gholamreza Nabiyouni [1]*, Kambiz Hedayati [2]

[1] *Department of Physics, Faculty of Science, Arak University, Arak, Iran*

[2] *Department of Science, Arak University of Technology, Arak, Iran*

ARTICLE INFO

ABSTRACT

In this article, $Ni_xMn_{1-x}Fe_2O_4$ ferrite nanoparticles were synthesized using surfactant free ultrasonic method, that x= 1, 0.75, 0.5, 0.25 and 0. The crystal structure of the synthesized nanoparticles was investigated using X-ray diffraction (XRD). It was found that they have a spinel structure. The crystallite size of the nanoparticles was also measured using Scherrer's relation. The morphology of nanoparticles was studied using scanning electron microscope (SEM). The magnetic properties and hysteresis loop of $Ni_xMn_{1-x}Fe_2O_4$ ferrites were investigated using vibrating sample magnetometer (VSM). The value of coercivity, saturation magnetization and remanent magnetization of the samples were calculated. In order to investigate the photocatalytic properties of the synthesized nanoparticles, the effect of particle on degradation of azo dyes acid brown and acid blue was studied. Based on the absorption spectrum obtained from the UV-Vis spectrometer, the amount of degradation of azo dyes by each of the nanoparticles were obtained at different times of UV irradiation.

INTRODUCTION

Ferrites are hard and brittle ferromagnetic materials. The general formula of ferrites can be written as $M(Fe_xO_y)$, where M is a bivalent metal such as nickel, manganese, copper, barium, yttrium, etc. Ferrites are polycrystalline materials and are composed of many small crystals with different orientations. In terms of crystal structure, ferrites are divided into four general categories: hexagonal, spinel, garnet and perovskite ferrites [1-3].

The general formula of spinel ferrites is $M(Fe_2O_4)$, where M is a metal such as: manganese, nickel, cobalt, zinc, copper or magnesium. In spinel ferrites, the crystal direction does not affect the magnetization of the material, and for this cause, they are considered as soft magnetic material. These ferrites are used in equipment that create alternating magnetic fields, such as microelectronic devices and the transformer cores and telecommunication inductors. Spinel materials are mainly classified into three categories: normal, inverted and complex spinel. The structure of ferro-spinel depends on the external electron configuration, divalent cation radius and the distribution of cations in different places. For example, $NiFe_2O_4$ is inverted spinel and $MnFe_2O_4$ is random spinel. The direction of the magnetic moment of the cations in the tetrahedral site A is opposite to the octahedral site B. Therefore,

* Corresponding Author Email: g-nabiyouni@araku.ac.ir

the magnetic moment of spinel ferrites can be adjusted by distributing different divalent cations in different places [4-6].

Polycrystalline spinel ferrites are widely used in the field of high-density magneto-optical recording devices, catalytic applications, magnetic separation, ferrofluids, targeted drug delivery, color imaging, magnetic refrigeration, gas sensing devices due to their chemical stability, high permeability in the radio frequency domain as well as high electrical and mechanical resistance [7-9].

What method is used to make spinel ferrite has a great effect on the chemical, structural and magnetic properties of that ferrite. Nickel, manganese, and combined ferrites of these two materials are made in different procedures, such as ultrasonic, co-precipitation, sol-gel, hydrothermal, auto-combustion, hydrothermal or hydrothermal coupled with a reverse micelle method, sonochemical method or microwave method [10-13].

Ultrasonic waves can lead to a better distribution of particles in the liquid, increase the rate of chemical reactions, reduce the reaction time, and also stimulate chemical reactions that do not occur in the absence of ultrasonic waves. In the synthesis of nanoparticles by the ultrasonic method, the reaction is carried out in an aqueous environment, and the ultrasonic waves are irradiated into the liquid and cause the atoms and molecules to vibrate. As a result of tensile stress and negative pressure caused by it, bubbles are formed in the liquid. The temperature and pressure inside these bubbles are very high and they have a half-life of nanoseconds. At the junction of these bubbles and the liquid, the water hydrolysis reaction has been carried out and due to the production of free radicals, the desired reactions for the production of nanostructures will occur. The higher the power of the ultrasonic device or the longer the duration of the wave radiation, the smaller the size of the synthesized nanoparticles [14-16].

Today, due to industrial advances, various toxic pollutants are produced, among which dyes can be mentioned. Dyes are synthetic and non-degradable organic compounds that dissolve in water. As a result, they can leave harmful effects on the environment and public health by polluting the water. An effective method for purifying
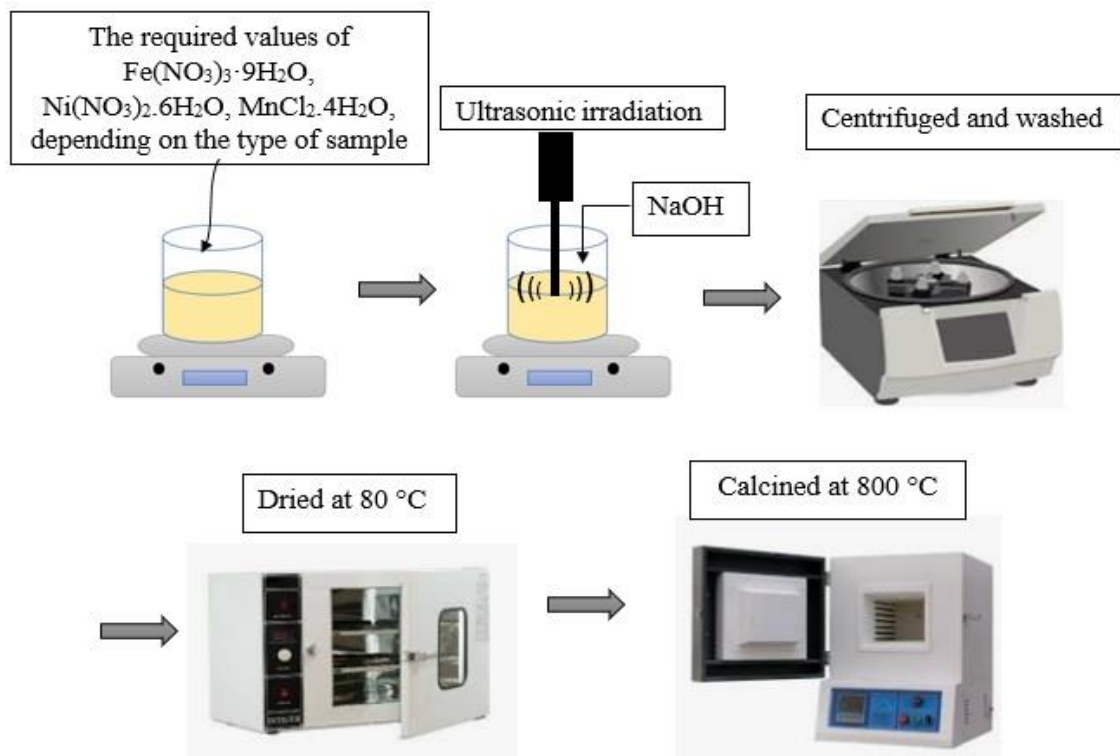
Fig. 1. Schematic of $Ni_xMn_{1-x}Fe_2O_4$ preparation nanocomposite preparation.

polluted water is using photocatalytic degradation. Photocatalysts are a group of catalysts that are activated by light and produce electron and hole pairs. These pairs can react with the molecules on the surface of the material and produce free radicals or strong oxidants and destroy organic compounds. If complete destruction is done, eventually water, carbon dioxide and inorganic compounds are produced during this process. Among the advantages of this method, we can mention the high speed of destruction, conversion

of toxic organic compounds into safe substances and working in environmental conditions. if the photocatalyst material has a high band gap, it is activated only by UV radiation. Today, we are mainly looking for photocatalysts that work with sunlight. The next point is related to separating the catalyst from the aqueous solution so that it can be used again. Magnetic ferrites have found wide applications in this branch of technology due to their low band gap and ability to be separated from the composition after the destruction
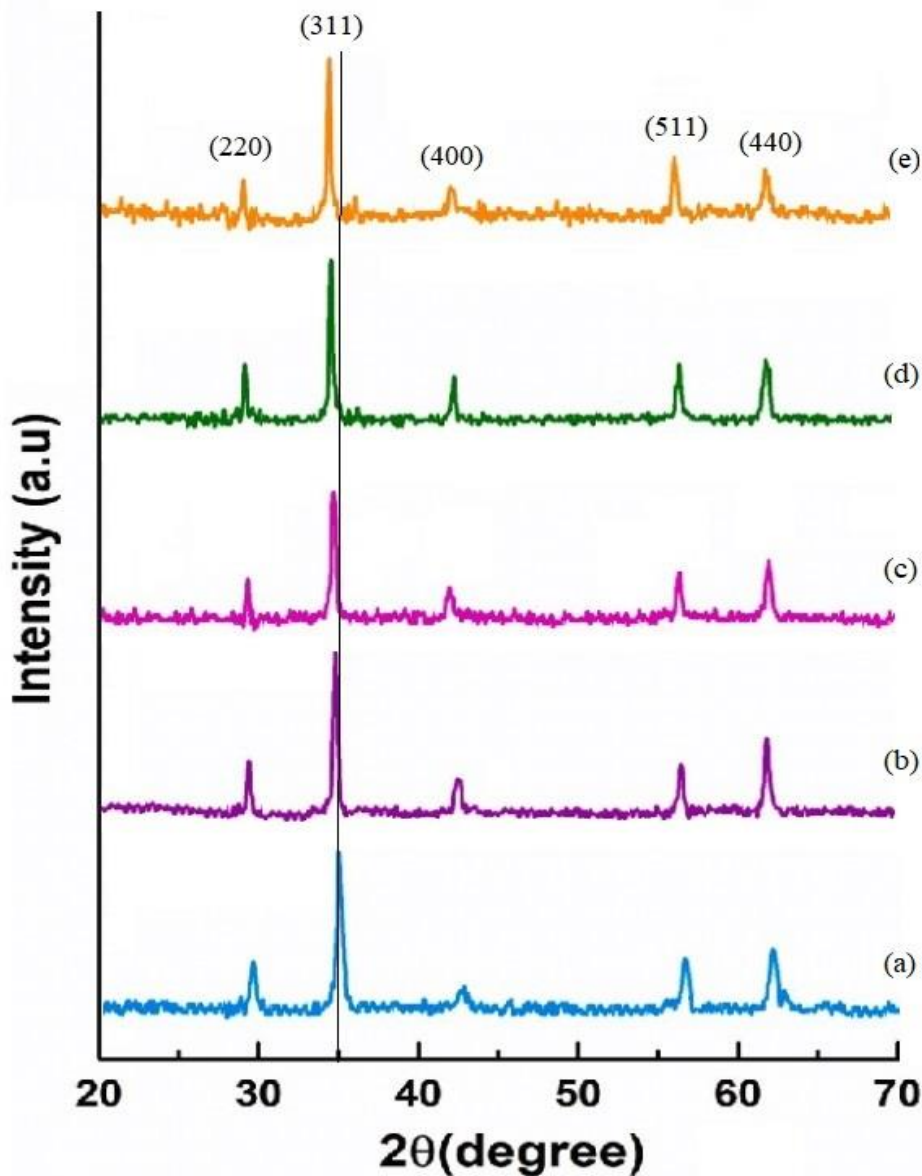
Fig. 2. XRD patterns of $Ni_xMn_{1-x}Fe_2O_4$ for a) x=1, b) x=0.75, c) x=0.5, d) x= 0.25, and x=0.

process by a magnetic field [17-19].

MATERIALS AND METHODS

Fe(NO$_3$)$_3$·9H$_2$O, Ni(NO$_3$)$_2$.6H$_2$O, MnCl$_2$.4H$_2$O, NaOH, acid brown, acid blue and deionized water, were used to synthesize nanoparticles. All chemicals were manufactured by Merck company and have a purity of 99.9%.

An ultrasonic device with a power of 1200 W and a titanium probe was used to generate ultrasonic waves and synthesize nanoparticles (Frafan Tajhiz Co, 20 kHz– 1200 W). A field emission scanning electron microscope (FESEM) was used to study the morphology of particles (LMU TESCAN BRNO-Mira3). X-ray diffraction patterns were obtained by Phillips model PW3040 device with Cu-Kα radiation 1.54 Å, in order to investigate the structural characteristics of nanoparticles. Room temperature magnetic properties of the samples were measured by Vibrating Sample Magnetometer (VSM: Meghnatis Kavir Kashan Co) . UV-Vis absorption spectrum of ferrite samples was recorded by using UV-Vis instrument in the wavelength range of 200-800 nm (Thermo Co, model Evolution 220).

In this work, NiFe$_2$O$_4$, Ni$_{0.75}$Mn$_{0.25}$Fe$_2$O$_4$, Ni$_{0.5}$Mn$_{0.5}$Fe$_2$O$_4$, Ni$_{0.25}$Mn$_{0.75}$Fe$_2$O$_4$ and MnFe$_2$O$_4$ ferrite nanoparticles were fabricated and studied. For this purpose, in the first step, for samples 1 to 5, Ni(NO$_3$)$_2$.6H$_2$O, MnCl$_2$.4H$_2$O and Fe(NO$_3$)$_3$·9H$_2$O in double distilled water with molar ratios of 1:0:2, 0.75:0.25:2, 0.5:0.5:2 and 0:1:2 were dissolved, respectively. After making the desired solutions, each sample was individually exposed to ultrasound radiation with an irradiation duration of 0.2 second pulses and the rest period of 0.1 second. Every 1 minute, 1 cc of NaOH (1 M) was added to the solution drop by drop, until the pH value reaches to 11. The resulting material was then centrifuged and washed well with double distilled water. All these steps were done at room temperature. Then it was placed in the oven at 80°C for 48 hours to dry. Finally, in order to improve the structural and magnetic properties, the sample was calcined for 2 hours in a furnace with a temperature of 800°C. Fig. 1 shows a schematic of the test steps.

RESULT AND DISCUSSION

The crystal structure of Ni$_x$Mn$_{1-x}$Fe$_2$O$_4$ ferrite nanoparticles was investigated by X-ray diffraction. The XRD patterns for x=1, 0.75, 0.5, 0.25 and 0 are shown in Figs. 2 (a-e) respectively. According
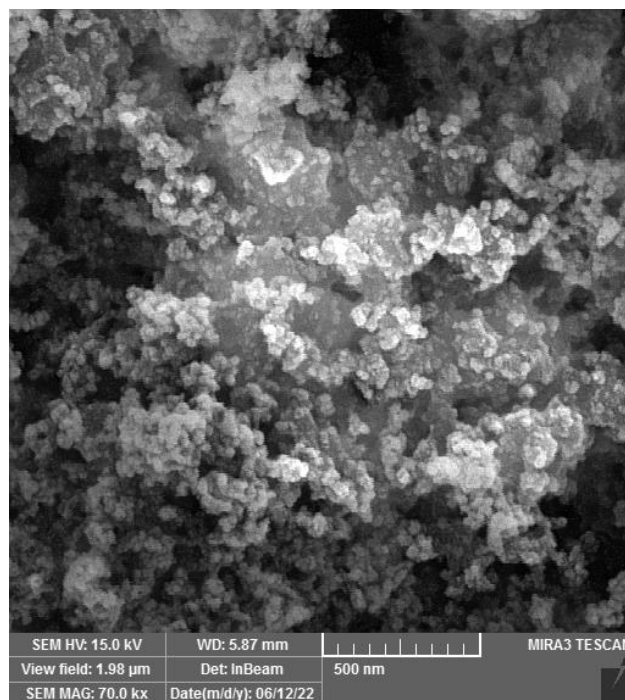
Fig. 3. SEM image of NiFe$_2$O$_4$ nanoparticles.

to the JCPDS No.: 03-0875, the NiFe$_2$O$_4$ ferrite nanoparticles have cubic structure with the lattice parameter of 8.34 nm. The MnFe$_2$O$_4$ nanoparticles (JCPDS No.: 75-0035) have cubic structure with the lattice parameter of 8.51 nm. Due to the fact that NiFe$_2$O$_4$ and MnFe$_2$O$_4$ have the same crystal structure, the Ni$_x$Mn$_{1-x}$Fe$_2$O$_4$ ferrites also have similar crystal structure with the same peaks. However, since the lattice parameter of MnFe$_2$O$_4$ is greater than which for NiFe$_2$O$_4$, by increasing the
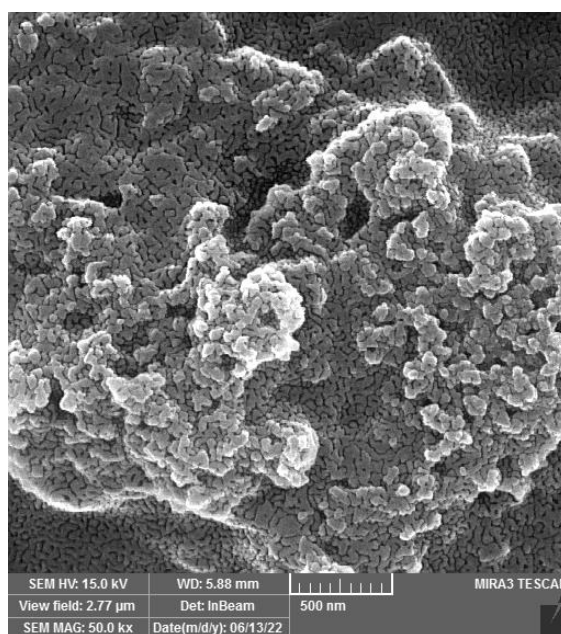
Fig. 4. SEM image of Ni$_{0.75}$Mn$_{0.25}$Fe$_2$O$_4$ nanoparticles.
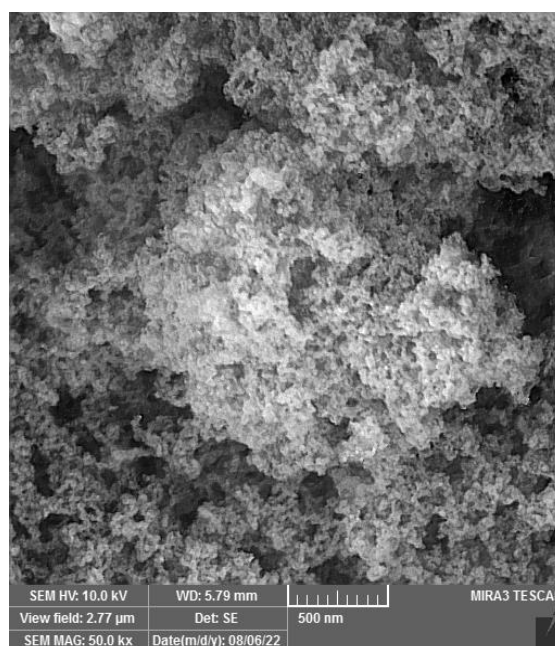
Fig. 5. SEM image of Ni$_{0.5}$Mn$_{0.5}$Fe$_2$O$_4$ nanoparticles.

amount of Mn in the ferrites, the peaks shift to the msaller wavelengths.

The crystalline sizes of $Ni_xMn_{1-x}Fe_2O_4$ ferrites

calculated by Scherrer equation ($D=0.9\lambda/\beta Cos\theta$), where β is FWHM, θ is diffraction position and λ is the X-ray wavelength (0.154 nm) [20]. The
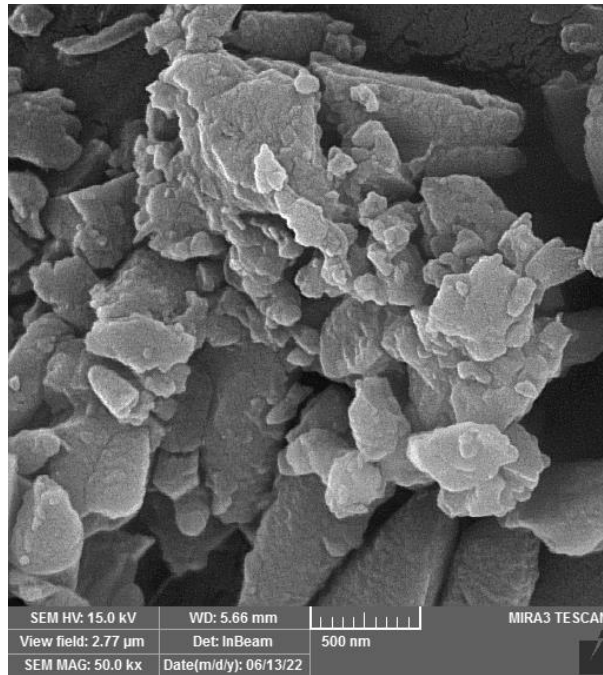
Fig. 6. SEM image of $Ni_{0.25}Mn_{0.75}Fe_2O_4$ nanoparticles.
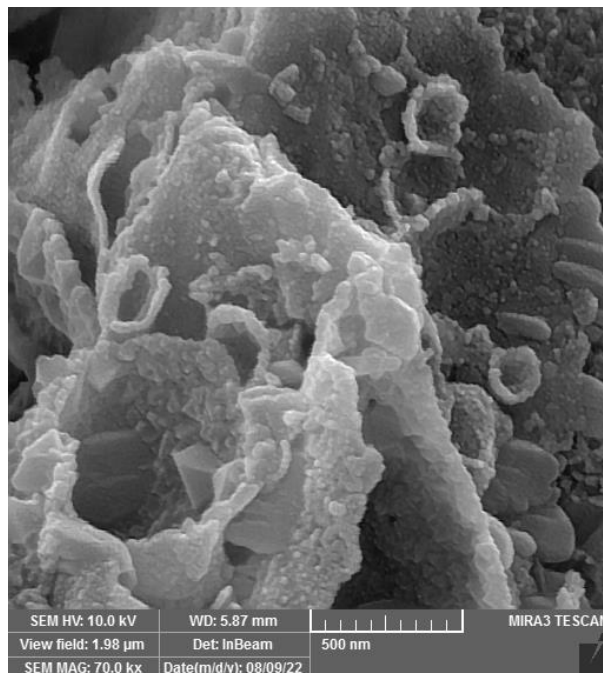
Fig. 7. SEM image of $MnFe_2O_4$ nanoparticles.

average crystalline size of $Ni_xMn_{1-x}Fe_2O_4$ ferrite nanoparticles for x=1, 0.75, 0.5, 0.25 and 0 were found to be about 28, 36, 22, 41 and 45 nm respectively.

SEM images of $Ni_xMn_{1-x}Fe_2O_4$ ferrites nanoparticles for x=1, 0.75, 0.5, 0.25 and 0 are shown in Figs. 3 -7, respectively.

As can be seen from the images, the nanoparticles are agglomerated, which can be due to the magnetic properties of the nanoparticles. Also, $Ni_{0.5}Mn_{0.5}Fe_2O_4$ nanoparticles have the smallest particle sizes compare with which for $MnFe_2O_4$ nanoparticles, which is consistent with the results obtained from Scherrer equation. The normalized magnetic hysteresis loops for $Ni_xMn_{1-x}Fe_2O_4$ for x=0, 0.25, 0.5, 0.75, and 1 are shown in Figs. 8 (a-e) respectively. The graphs show, all nanoparticles have soft ferromagnetic properties.

The coercivity plot of $Ni_xMn_{1-x}Fe_2O_4$ nanoparticles vs x amount is shown in Fig. 9. This diagram shows that coercivity of $NiFe_2O_4$ sample is higher than which for $MnFe_2O_4$. The presence
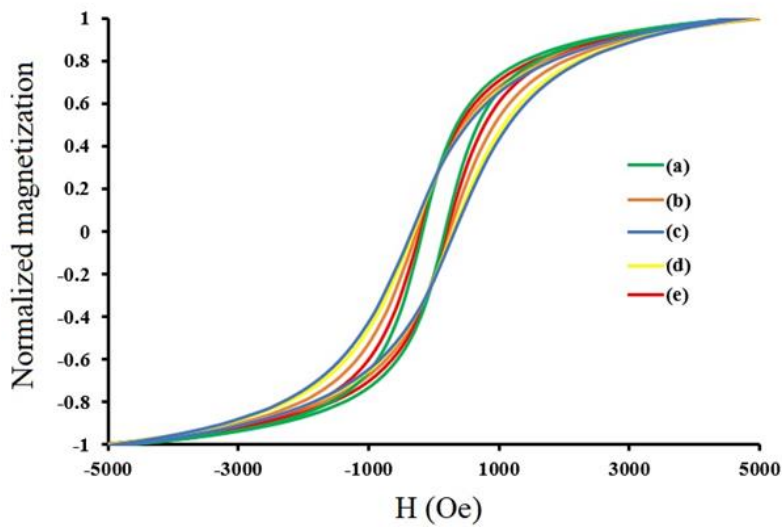
Fig. 8. The hysteresis loops of $Ni_xMn_{1-x}Fe_2O_4$ nanoparticles for a) x=0, b) x=0.25, c) x=0.5, d) x= 0.75, and e) x=1.
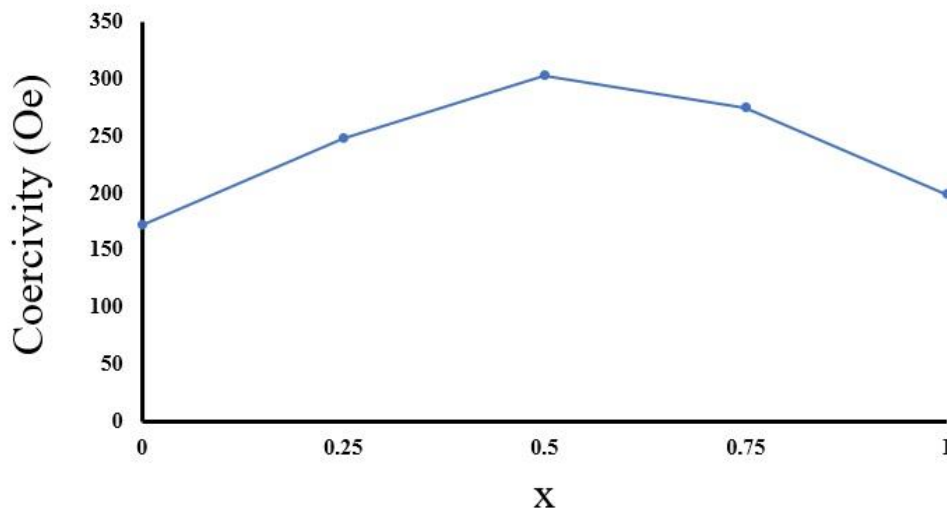
Fig. 9. Coercivity plot of $Ni_xMn_{1-x}Fe_2O_4$ nanoparticles vs the x amount.

of impurities in NiFe$_2$O$_4$ or MnFe$_2$O$_4$ ferrites leads to increase the coercivity values. Due to the fact that the Ni$_{0.5}$Mn$_{0.5}$Fe$_2$O$_4$ sample has the highest impurity, it has also a higher coercivity compare with the other ferrites.

The UV–Vis absorption spectra of pure acid blue is given in Fig. 10 a. The absorption diagram of acid blue in the presence of Ni$_x$Mn$_{1-x}$Fe$_2$O$_4$ ferrite

nanoparticles for x=1, 0.75, 0.5, 0.25 and 0 after being exposed to UV irradiation for 60 minutes are shown in Figs. 10 (b-f) respectively. As can be seen in these figures, MnFe$_2$O$_4$ has a higher degradation rate than NiFe$_2$O$_4$. Also, by adding impurities to the ferrites and forming a combined ferrite, the amount of destruction increases, which can be due to the creation of intermediate levels.
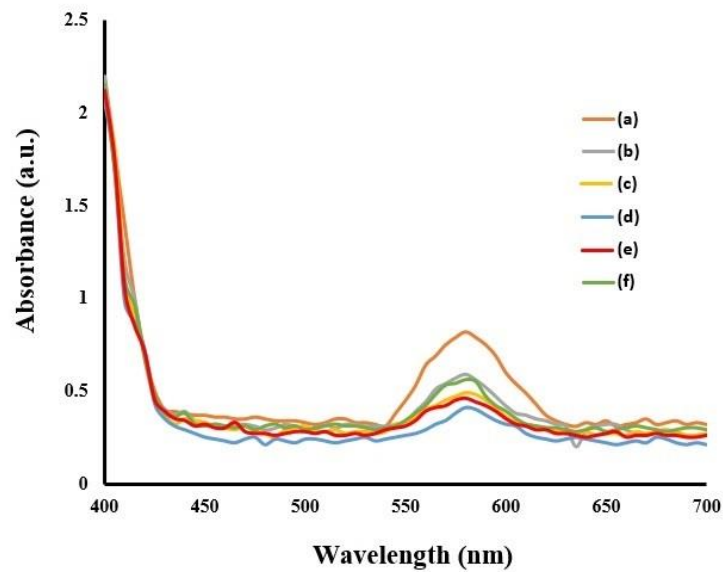
Fig. 10. UV–Vis absorption spectra of a) pure acid blue and acid blue in the presence of Ni$_x$Mn$_{1-x}$Fe$_2$O$_4$ for b) x=1, c) x=0.75, d) x=0.5, e) x=0.25, and f) x=0 after 1 h of UV irradiation.
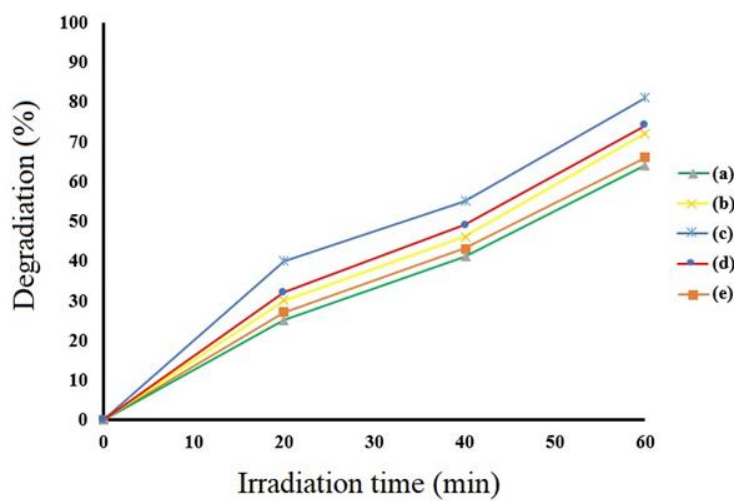
Fig. 11. Degradation percent versus UV irradiation time for acid blue in the presence of Ni$_x$Mn$_{1-x}$Fe$_2$O$_4$ for b) x=1, c) x=0.75, d) x=0.5, e) x=0.25, and f) x=0.

The degradation percentages vs UV irradiation times for acid blue in the presence of $Ni_xMn_{1-x}Fe_2O_4$ (x=1, 0.75, 0.5, 0.25, and 0) are given in Figs. 11. The rate of degradation over time is more or less similar for all ferrite samples.

The absorption spectra of pure acid brown is shown in Fig. 12 a. The Figs. 12 (b-f) give the absorption graph of acid brown in the presence

of $Ni_xMn_{1-x}Fe_2O_4$ nanoparticles (x=1, 0.75, 0.25, and 0), for 60 minutes UV irradiation. The degradation of each sample for acid brown is similar to which for acid blue.

The graphs of degradation in terms of time for acid brown in the presence of $Ni_xMn_{1-x}Fe_2O_4$ nanoparticles for x=1, 0.75, 0.5, 0.25 and 0 is shown in Fig. 13, respectively. These results are
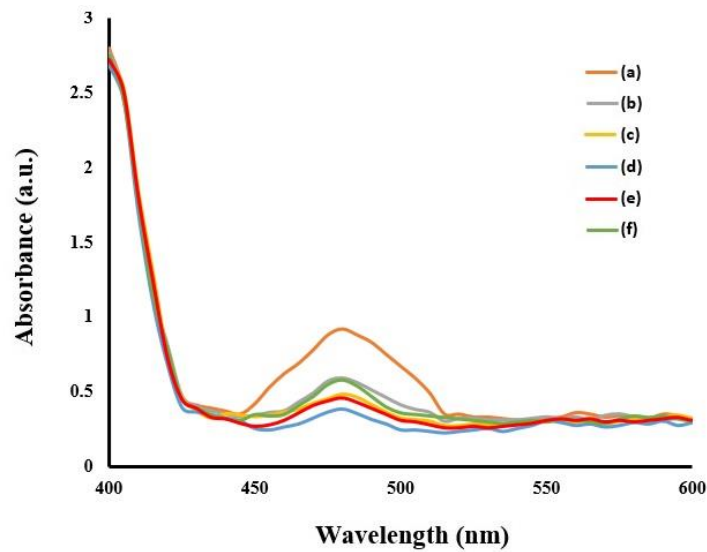
Fig. 12. UV–Vis absorption spectra of a) pure acid brown and acid brown in the presence of $Ni_xMn_{1-x}Fe_2O_4$ for b) x=1, c) x=0.75, d) x=0.5, e) x=0.25, and f) x=0 after 1 h of UV irradiation.
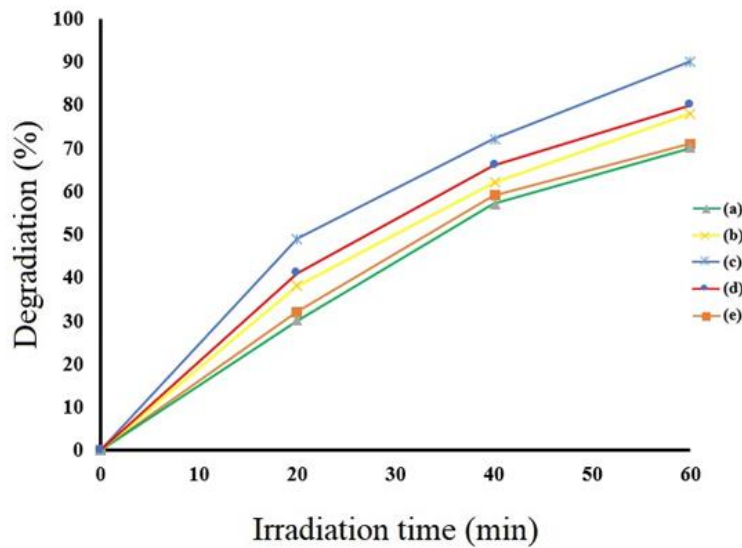
Fig. 13. Degradation percent versus UV irradiation time for acid brown in the presence of $Ni_xMn_{1-x}Fe_2O_4$ for b) x=1, c) x=0.75, d) x=0.5, e) x=0.25, and f) x=0.

the similar as which give in Fig. 11. for acid blue.

CONCLUSION

In this research, Ni$_x$Mn$_{1-x}$Fe$_2$O$_4$ nanoparticles were synthesized using ultrasonic method. X-ray diffraction examined the crystal structure of nanoparticles and showed that all samples have a cubic structure. Since the lattice parameter of MnFe$_2$O$_4$ is greater than which for NiFe$_2$O$_4$, a shift to shorter wavelengths is observed as the value of x decreases. Scherrer equation and SEM images show that Ni$_{0.5}$Mn$_{0.5}$Fe$_2$O$_4$ nanoparticles have the smallest particle size and MnFe$_2$O$_4$ nanoparticles have the largest particle size. The coercivity of NiFe$_2$O$_4$ has the higher value than which for MnFe$_2$O$_4$. Also, the presence of impurities in the ferrite increases the coercivity value and the Ni$_{0.5}$Mn$_{0.5}$Fe$_2$O$_4$ has the highest coercivity. For both brown and blue acids azo dyes, NiFe$_2$O$_4$ has the lowest amount of degradation, while when the amount of Mn and Ni in Ni$_x$Mn$_{1-x}$Fe$_2$O$_4$ is equal, the highest degradation is observed.

CONFLICT OF INTEREST

The authors declare that there is no conflict of interests regarding the publication of this manuscript.

REFERENCES

1. Tatarchuk TR, Bououdina M, Paliychuk ND, Yaremiy IP, Moklyak VV. Structural characterization and antistructure modeling of cobalt-substituted zinc ferrites. J Alloys Compd. 2017;694:777-791.
2. Houbi A, Aldashevich ZA, Atassi Y, Bagasharova Telmanovna Z, Saule M, Kubanych K. Microwave absorbing properties of ferrites and their composites: A review. J Magn Magn Mater. 2021;529:167839.
3. Thakur P, Chahar D, Taneja S, Bhalla N, Thakur A. A review on MnZn ferrites: Synthesis, characterization and applications. Ceram Int. 2020;46(10):15740-15763.
4. Ma J, Zhao B, Xiang H, Dai F-Z, Liu Y, Zhang R, et al. High-entropy spinel ferrites MFe$_2$O$_4$ (M = Mg, Mn, Fe, Co, Ni, Cu, Zn) with tunable electromagnetic properties and strong microwave absorption. Journal of Advanced Ceramics. 2022;11(5):754-768.
5. Carpenter G, Sen R, Malviya N, Gupta N. Microwave-assisted synthesis and characterization of nickel ferrite nanoparticles. AIP Conference Proceedings: AIP Publishing LLC; 2015. p. 020029.
6. Qindeel R, Alonizan NH. Structural, dielectric and magnetic properties of cobalt based spinel ferrites. Current Applied Physics. 2018;18(5):519-525.
7. Smitha P, Singh I, Najim M, Panwar R, Singh D, Agarwala V, et al. Development of thin broad band radar absorbing materials using nanostructured spinel ferrites. Journal of Materials Science: Materials in Electronics. 2016;27(8):7731-7737.
8. Mathew DS, Juang R-S. An overview of the structure and magnetism of spinel ferrite nanoparticles and their synthesis in microemulsions. Chem Eng J. 2007;129(1-3):51-65.
9. Kefeni KK, Mamba BB, Msagati TAM. Application of spinel ferrite nanoparticles in water and wastewater treatment: A review. Sep Purif Technol. 2017;188:399-422.
10. Gyergyek S, Makovec D, Kodre A, Arčon I, Jagodič M, Drofenik M. Influence of synthesis method on structural and magnetic properties of cobalt ferrite nanoparticles. J Nanopart Res. 2009;12(4):1263-1273.
11. Lungu A, Malaescu I, Marin CN, Vlazan P, Sfirloaga P. The electrical properties of manganese ferrite powders prepared by two different methods. Physica B: Condensed Matter. 2015;462:80-85.
12. Behnia B, Safardoust-Hojaghan H, Amiri O, Salavati-Niasari M, Anvari AA. High-performance cement mortars-based composites with colloidal nano-silica: Synthesis, characterization and mechanical properties. Arab J Chem. 2021;14(9):103338.
13. Harzali H, Saida F, Marzouki A, Megriche A, Baillon F, Espitalier F, et al. Structural and magnetic properties of nano-sized NiCuZn ferrites synthesized by co-precipitation method with ultrasound irradiation. J Magn Magn Mater. 2016;419:50-56.
14. Abbasian AR, Lorfasaei Z, Shayesteh M, Afarani MS. Synthesis of cobalt ferrite colloidal nanoparticle clusters by ultrasonic-assisted solvothermal process. Journal of the Australian Ceramic Society. 2020;56(3):1119-1126.
15. Malaescu I, Lungu A, Marin CN, Vlazan P, Sfirloaga P, Turi GM. Experimental investigations of the structural transformations induced by the heat treatment in manganese ferrite synthesized by ultrasonic assisted co-precipitation method. Ceram Int. 2016;42(15):16744-16748.
16. Chen D, Li D-y, zhang Y-z, Kang Z-t. Preparation of magnesium ferrite nanoparticles by ultrasonic wave-assisted aqueous solution ball milling. Ultrason Sonochem. 2013;20(6):1337-1340.
17. Casbeer E, Sharma VK, Li X-Z. Synthesis and photocatalytic activity of ferrites under visible light: A review. Sep Purif Technol. 2012;87:1-14.
18. Ismael M. Ferrites as solar photocatalytic materials and their activities in solar energy conversion and environmental protection: A review. Sol Energy Mater Sol Cells. 2021;219:110786.
19. Behnia B, Anvari AA, Safardoust-Hojaghan H, Salavati-Niasari M. Positive effects of novel nano-zirconia on flexural and compressive strength of Portland cement paste. Polyhedron. 2020;177:114317.
20. Hedayati K, Nabiyouni G. Surface roughness analysis and magnetic property studies of nickel thin films electrodeposited onto rotating disc electrodes. Appl Phys A. 2014;116(4):1605-1612.